https://doi.org/10.5194/gmd-2021-347
Preprint. Discussion started: 10 December 2021

Geoscientific Model Development Discussions

Simulation Model of Reactive Nitrogen Species in an Urban Atmosphere using a Deep Neural Network: RNDv1.0

Junsu Gil[1], Meehye Lee[1*], Jeonghwan Kim[2], Gangwoong Lee[2], Joonyoung Ahn[3]

[1] *Department of Earth and Environmental Science, Korea University, Seoul, South Korea*

[2] *Department of Environmental Science, Hankuk University of Foreign Studies, Yongin, South Korea*

[3] *Air Quality Forecasting Center, Climate and Air Quality Research Department, National Institute of Environmental Research (NIER), Incheon, South Korea*

* *Corresponding author*: Meehye Lee (meehye@korea.ac.kr)

Abstract

Nitrous acid (HONO), one of the reactive nitrogen oxides (NO_y), plays an important role in the formation of ozone (O_3) and fine aerosols ($PM_{2.5}$) in the urban atmosphere. In this study, a simulation model of Reactive Nitrogen species using Deep neural network model (RND) was constructed to calculate the HONO mixing ratios through a deep learning technique using measured variables. A Python-based Deep Neural Network (DNN) was trained, validated, and tested with HONO measurement data obtained in Seoul during the warm months from 2016 to 2019. A k-fold cross validation and test results confirmed the performance of RND v1.0 with an Index Of Agreement (IOA) of 0.79 ~ 0.89 and a Mean Absolute Error (MAE) of 0.21 ~ 0.31 ppbv. The RNDV1.0 adequately represents the main characteristics of HONO and thus, RND v1.0 is proposed as a supplementary model for calculating the HONO mixing ratio in a high-NO_x environment.

1. Introduction

Reactive nitrogen oxides (NO_y) plays an important role in critical environmental issues concerning the Earth's atmosphere, spanning from local air pollution to global climate change (Sun et al., 2011;Ge et al., 2019). The oxidation of NO to NO_2, and finally to HNO_3, is the backbone of the chemical mechanism producing ozone (O_3) and $PM_{2.5}$ (particulate matter of size ≤ 2.5 μm), and determines the oxidization capacity of the atmosphere. However, observational constraints on individual species limit the understanding of key mechanisms and, consequently, problem solving. In the atmosphere, NO_y is a family of nitrogenous compounds including NO_x (=NO + NO_2), HONO, NO_3, HNO_3, organic nitrates (e.g., PAN), and particulate NO_3^-. These species are produced and recycled through photochemical reactions until they are removed through wet or dry deposition (Liebmann et al., 2018;Brown et al., 2017;Wang et al., 2020;Li et al., 2020). In recent years, the NO_y cycle has drawn increased attention because of the heterogeneous reactions leading to O_3 and $PM_{2.5}$ formation (Brown et al., 2017). Modeling studies have also shown that the lack of NO_y measurements hinder a comprehensive understanding of the heterogeneous reactions (Anderson et al., 2014;Wang et al., 2017b;Chen et al., 2018).

HONO, one of the NO_y species, is an early morning source of OH radicals in the urban atmosphere (Brandenburger et al., 1998;Xing et al., 2019;Alicke et al., 2002;Ryan et al., 2018;Gil et al., 2020;Xue et al., 2020). Thus, there has been a steady effort to determine the atmospheric level of HONO using various methods such as a long path absorption photometer (LOPAP) (Kleffmann et al., 2006;Xue et al., 2019), chemical ionization mass spectrometry (CIMS) (Levy et al., 2014;Roberts et al., 2010), ion chromatography (IC) (VandenBoer et al., 2014;Gil et al., 2020;Ye et al., 2016;Xu et al., 2019), and quantum cascade tunable infrared laser differential absorption spectrometry (QC-TILDAS) (Lee et al., 2011;Gil et al., 2021). These studies have reported a considerable level of HONO in the early morning. On the other hand, the model results are still significantly lower than the levels observed in big cities such as Beijing, where HONO formation involving various surfaces is a major contributor in this underestimation (Liu et al., 2019).

Recently, a multi-layer artificial neural network, referred to as a Deep Neural Network (DNN), has been adopted in the atmospheric sciences because of its powerful ability to process large amounts of data, allowing improvements in the performance of conventional models (Reichstein et al., 2019;Cui and Wang, 2021). DNN employs a statistical method to obtain the optimum solution for the target species without prior information on the physicochemical processes. In this study, we aimed to develop a user-friendly Reactive Nitrogen species simulation model using simple DNN (RND) based on ground measurements in a highly polluted urban area. Since this is the first attempt to calculate HONO mixing ratios using a first version of RND model (RNDv1.0), we describe the entire modeling process and evaluate the model results by comparing them with the measurements.

2. Model description

The development of RNDv1.0 model follows the systematic steps including collecting data, preprocessing data, building the DNN, training and validating the model, and testing the performance of the model (Figure 1). The RNDv1.0 was written in Python and necessary libraries to build and operate RNDv1.0 are listed in Table 1.

2.1. Collection of measurement data

As the first step constructing the RNDv1.0, measurement data were obtained including HONO, reactive gases, and meteorological parameters. The HONO mixing ratio was measured using a Quantum Cascade – Tunable Infrared Laser Differential Absorption Spectrometer (QC-TILDAS) system in Seoul during May–June 2016, June 2018, and April-June 2019 (Lee et al., 2011;Gil et al., 2021). When testing and evaluating atmospheric HONO measurement methods, QC-TILDAS has been chosen as the reference method for comparing ambient HONO mixing ratios measured using several different techniques owing to its advantages of low detection limits (~ 0.1 ppbv) and high temporal resolution (Pinto et al., 2014). More details on measurements can be found elsewhere (Gil et al., 2021). HONO was measured at Olympic Park (37.52°N, 127.12°E) during the Korea-United States Air Quality (KORUS-AQ) study in 2016 (Kim et al., 2020;Gil et al., 2021), at the campus of Korea University in 2018 (37.59°N, 127.03°E), and at the site near the campus in 2019 (37.59°N, 127.08°E) (NIER, 2020) (Figure S1). Of the three sites, the Korea University campus and Olympic Park have served as

https://doi.org/10.5194/gmd-2021-347
Preprint. Discussion started: 10 December 2021

measurement sites representing the air quality of Seoul. In fact, it has been known that O_3 and $PM_{2.5}$ levels are strongly influenced by the synoptic circulation throughout the Korean peninsula (Peterson et al., 2019;Jordan et al., 2020). In addition, trace gases including O_3, NO_2, CO, and SO_2 and meteorological parameters including temperature (T), relative humidity (RH), wind speed (WS) and direction (WD) were measured. The measurement statistics are presented in Table 2 and Table S1. Briefly summarizing, the 10th and 90th percentile mixing ratios of HONO, NO_2, and O_3 are 0.3 ppbv and 1.9 ppbv, 10.7 ppbv and 48.2 ppbv, and 12.0 ppbv and 80.9 ppbv, respectively for the entire experiment periods.

2.2. Preparation of input data

In the next step, the observation data set was prepared for RNDv1.0 model construction. As input variables, chemical and meteorological parameters are used, including the mixing ratios of O_3, NO_2, CO, and SO_2, along with temperature (T), relative humidity (RH), wind speed (WS), wind direction (WD), and solar zenith angle (SZA) to estimate the target species, HONO, as the output. Wind direction in degrees should be converted to a cosine value for continuity. For data integrity, there should be no missing values in the input dataset. Finally, 50.7 % of all arrays of available measurement data (1636) were used to construct the RNDv1.0 in this study.

Since the measurements of these nine variables vary over a wide range in different units, they were normalized to avoid bias during the calculations. Among the widely used normalization methods, '*min-max scaling*' method was adopted and input variables were normalized against the minimum and maximum values in this study (Eq. 1):

$$x_{sca} = \frac{x_{raw} - F_2(X)}{F_1(X)}, \quad (1)$$

where x_{raw} is raw data of input variable (X), x_{sca} is scaled data of X, F_1 and F_2 are scale factors of X, and are given for each input variable used in Table 2.

https://doi.org/10.5194/gmd-2021-347
Preprint. Discussion started: 10 December 2021

Geoscientific Model Development Discussions

2.3. Neural network architecture and hyperparameters

At this stage, the network is built to calculate HONO using those input variables. The RNDv1.0 is composed of five hidden layers (Figure 2), which employed an exponential linear unit (ELU) as an activation function (Eq. 2).

$$\text{ELU}: \phi(x) = \begin{cases} e^{x} - 1 \ (x < 0) \\ x \ (x \geq 0) \end{cases}. \tag{2}$$

In a DNN, an activation function creates a nonlinear relationship between an input variable and an output variable. When constructing a DNN model, an ELU has the advantage of a fast-training process and better performance in handling negative values than other activation functions (Wang et al., 2017a;Ding et al., 2018). In addition, the mean squared error and Adam optimizer were applied as loss function and optimize function, respectively. The learning rate, epoch, and batch were set to 0.01, 100, and 32, respectively.

2.4. Train and validation

The RNDv1.0 model was trained and validated with HONO measurements obtained during May ~ June in 2016 and 2019, and tested against those obtained in June 2018 and April 2019 (Figure 3). The number of data used for train and validation, and test were 1122 and 514, respectively.

With the hyperparameters specified in previous section, the performance of the model was validated using the k-fold cross-validation method, which is especially useful when the size of dataset is small (Bengio and Grandvalet, 2003). In the k-fold cross-validation method (Figure 3), the entire data is randomly divided into k subsets, of which k-1 sets were used for training and the rest one was used for validation. k was set to 5 in this study. The accuracy was determined by Index Of Agreement (IOA) and Mean Absolute Error (MAE) expressed by the following equation (Eq. 3, Eq. 4):

$$\mathrm{IOA} = 1 - \frac{\sum_{i=1}^{n}(O_i - P_i)^2}{\sum_{i=1}^{n}(|P_i - \bar{O}| + |O_i - \bar{O}|)^2}, \quad (3)$$

$$\mathrm{MAE} = \frac{\sum_{i=1}^{n}|O_i - P_i|}{n}, \quad (4)$$

where O_i, P_i, $\bar{O}$, and n are the observed value, predicted value, average of the observed values, and number of nodes, respectively. The overall accuracy of

As IOA and MAE vary according to the number of nodes, they were calculated for the measured ($HONO_{obs}$) and calculated ($HONO_{mod}$) mixing ratios by varying the number of nodes from 0 to 100 in each hidden layer. The best performance was found with 41 nodes, with which the averaged IOA and MAE were 0.89 ± 0.01 (mean ± standard deviation) and 0.31 ± 0.02 ppbv, respectively (Figure 4). The high level of IOA and low MAE demonstrates that the performance of RNDv1.0 model is adequate, and it is capable of simulating the ambient HONO mixing ratio using the routinely measured chemical and meteorological parameters. In particular, MAE was commensurate with the detection limit of HONO measurement.

After the network validation, HONO mixing ratio was calculated for May ~ June in 2016 and 2019, and the model results were compared with the measured values (Figure 5). The average mixing ratios of measured and calculated HONO was 0.94 ppbv and 0.89 ppbv in 2016, and 1.02 ppbv and 0.96 ppbv in 2019, respectively. The MAE and IOA of the measurement and calculation were 0.27 ppbv and 0.90 in 2016, and 0.29 ppbv and 0.91 in 2019, respectively, demonstrating the ability of the RNDv1.0 to simulate ambient HONO levels. In both cases, however, the model slightly underestimated the highest and lowest HONO mixing ratios, which is mainly due to the limited number of data used for training, but also related to the intrinsic nature of DNN. The model calculation well captured the diurnal variation of ambient HONO with a slight underestimation (Figure 6). In addition, the correlation between $HONO_{mod}$ and $HONO_{obs}$ was better in 2019 (MAE = 0.06 ppbv) than in 2016 (MAE = 0.08 ppbv). Since the MAE of the two cases was far below the detection limit of HONO measurements (~ 0.1 ppbv), the RNDv1.0 is considered adequate to simulate HONO in urban areas.

2.5. Performance test

https://doi.org/10.5194/gmd-2021-347
Preprint. Discussion started: 10 December 2021

Finally, the RND model was tested against the measurement data obtained in June 2018 and April 2019. The calculated HONO mixing ratios are compared with those measured in Figure 7, and their MAE and IOA are listed in Table 3. The two sets of model performance test showed that the model reasonably traced what was observed. In June 2018, the MAE and IOA of the calculated and measured are comparable to those of validation. However, the MAE and IOA of the April 2019 measurements were relatively poor compared to the validation results. Especially, the MAE of the April 2018 is about twice as high as those of validation. In these two test periods, HONO levels were lower than those observed on validation days (Figure 5), and the model tended to overestimate high HONO concentrations, unlike in the validation case. The discrepancy is probably due to seasonality: the difference in meteorological and chemical regime of the atmosphere. For example, the monthly average temperature, relative humidity, and NO_2 mixing ratio of Seoul in 2019 were 12.1 ℃, 50.9 %, and 29 ppbv in April 2019 and 22.5 °C, 60.6 %, and 21 ppbv in June 2019 (https://cleanair.seoul.go.kr; https://weather.go.kr). Note that the RNDv1.0 model was trained with the 9 variables measured in early summer (Table 2). Therefore, the more measurement data spanning a full year for training, the more accurate the model estimates will be.

3. Operation and application of RNDv1.0

The RNDv1.0 package is provided as an operational model, .h5 files that can be opened in Python. To run the RNDv1.0, the measurement data for nine input variables are required and need to be properly prepared as described in Section 2.2. A sample of preprocessed input dataset is provided as a .csv file (Dataset_for_model.csv). Once the input data is ready, open the RND model with input data files using the code provided in the example (Figure S2). Then, RND v1.0 calculates and presents the HONO results as scaled values (x_{sca}), which will be finally converted to HONO mixing ratio (ppbv) by the two scale factors in Table 2 (Eq. 5):

$$\mathrm{HONO\ (ppbv)} = \mathrm{HONO_{sca}} \times \mathrm{F_1(HONO)} + \mathrm{F_2(HONO)}. \qquad (5)$$

https://doi.org/10.5194/gmd-2021-347
Preprint. Discussion started: 10 December 2021

Geoscientific Model Development
Discussions
Open Access
EGU

The result of the RNDv1.0, HONO, can be applied to an urban photochemical cycle simulation. It is already known that the photolysis of HONO is a major source of OH radicals in the early morning when the OH level is low, and this OH affects daytime O_3 formation through photochemical reactions with VOCs and NO_x, which are primarily emitted during morning rush hour in urban areas. Therefore, the OH produced from HONO expedites photochemical reactions, promoting O_3 formation. However, the HONO formation mechanism is still poorly understood, and concentrations are not correctly simulated in conventional photochemical models; therefore, the absence of HONO causes great uncertainty in O_3 prediction (Figure 8).

The 0-Dimension Atmospheric Modelling (F0AM) utilizing the MCM v3.3.1 chemical reaction mechanisms (Wolfe et al., 2016), can be used to simulate the diurnal variation of O_3 with the measurements of several reactive gases (NO, NO_2, CO, HCHO, VOCs, and HONO). Detailed information about F0AM can be found in (https://sites.google.com/site/wolfegm/models) and in previous works published elsewhere (Wolfe et al., 2016; Gil et al., 2020). When the F0AM model is run without HONO, it is not able to reproduce the concentration and diel cycle of the observed O_3 (Figure 8). In comparison, the model simulates the O_3 well within 2 ppbv when adding HONO, which is the product of RND v1.0. This is mainly due to the missing OH produced by HONO photolysis in the early morning. Its production rate is estimated to be 0.57 pptv s^{-1}, contributing approximately 2.28 pptv to OH budget during 06:00 ~ 11:00 (LST) (Gil et al., 2021). Given that OH is mainly produced from the photolysis of O_3 under high sun, the early morning source of OH will expedite the photochemical cycle involving NO_x and VOCs, promoting O_3 and secondary aerosol formation. Since the presence of HONO in the photochemical model allows for accurate estimation of OH radicals, the incorporation of RND into conventional models will improve their overall performance.

4. Summary and implications

In this study, we developed the RND model to calculate the mixing ratio of NO_y in an urban atmosphere using a DNN along with measurement data. The target species of RNDv1.0 is HONO, and its mixing ratio is calculated using trace gases including O_3, NO_2, CO, and SO_2, and meteorological variables including T, RH, WS, and WD, along with the SZA. These variables are routinely measured through monitoring networks. The RNDv1.0 was trained and validated using the HONO measurements obtained in Seoul by adopting a k-fold cross validation method and tested with other HONO datasets measured using the same instrument. The validation and test results demonstrate that RND adequately captures the characteristic variation of HONO and confirms the efficacy of RND v1.0.

RNDv1.0 was constructed using measurements made in a high NO_x environment during early summer (May–June). It is noteworthy that in this period, the HONO mixing ratio was raised above 3 ppbv with the highest O_3 levels under stagnant conditions. If RND is applied to areas under significant influence of outflows, the model possibly overestimates or underestimate the level of HONO without detailed information such as nanoparticles. In the previous study, the formation of HONO was shown to be intimately related with surface areas of submicron particles (Gil et al., 2021). Nevertheless, the HONO volume mixing ratio produced from simple codes in RNDv1.0 with routine measurements provides the benefit of relatively inexpensive test for the current knowledge of the urban photochemical cycle. Therefore, it is reasonable to argue that RND can serve as a supplementary tool for conventional photochemical models.

5. Acknowledgements

This study was financially supported by the National Research Foundation of Republic of Korea (2020R1A2C3014592).

6. Code availability

https://doi.org/10.5194/gmd-2021-347
Preprint. Discussion started: 10 December 2021

The RND model codes (.h5 files) with preprocessed sample data can be downloaded from (Gil, 2021).

7. Author contributions

JG and ML designed the manuscript and developed the model code. JK, GL, and JA provided the measurement data and validated the model. All the authors contributed to the manuscript.

8. Competing interests

The authors declare that they have no conflict of interest.

https://doi.org/10.5194/gmd-2021-347
Preprint. Discussion started: 10 December 2021

Figures and Tables

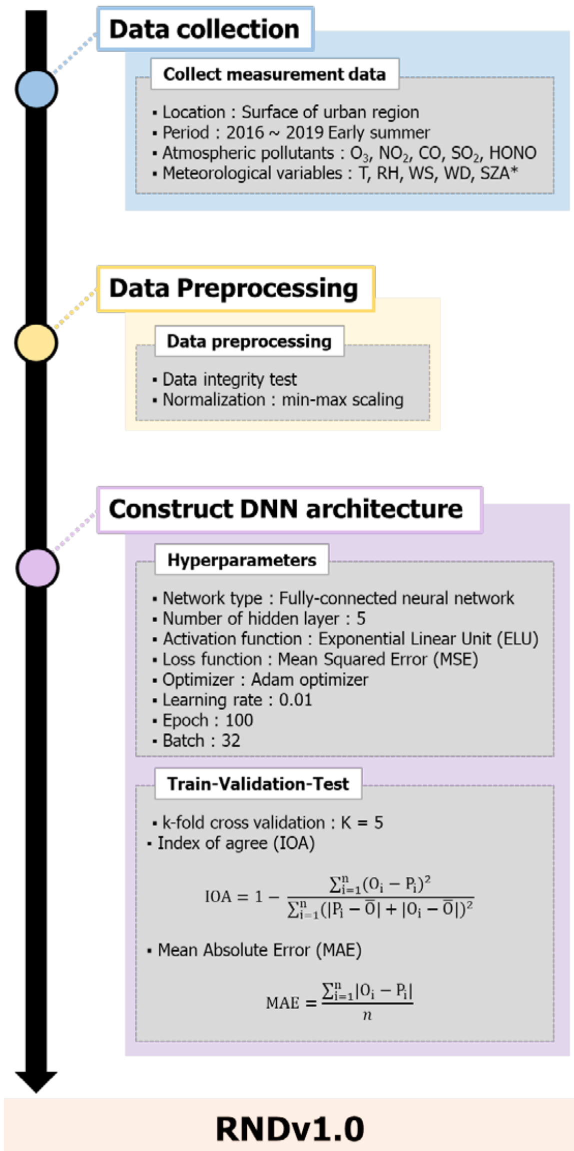

Figure 1. The main processes for configuring the RNDv1.0 (*: calculated values)

https://doi.org/10.5194/gmd-2021-347
Preprint. Discussion started: 10 December 2021

Geoscientific Model Development
Discussions
Open Access
EGU

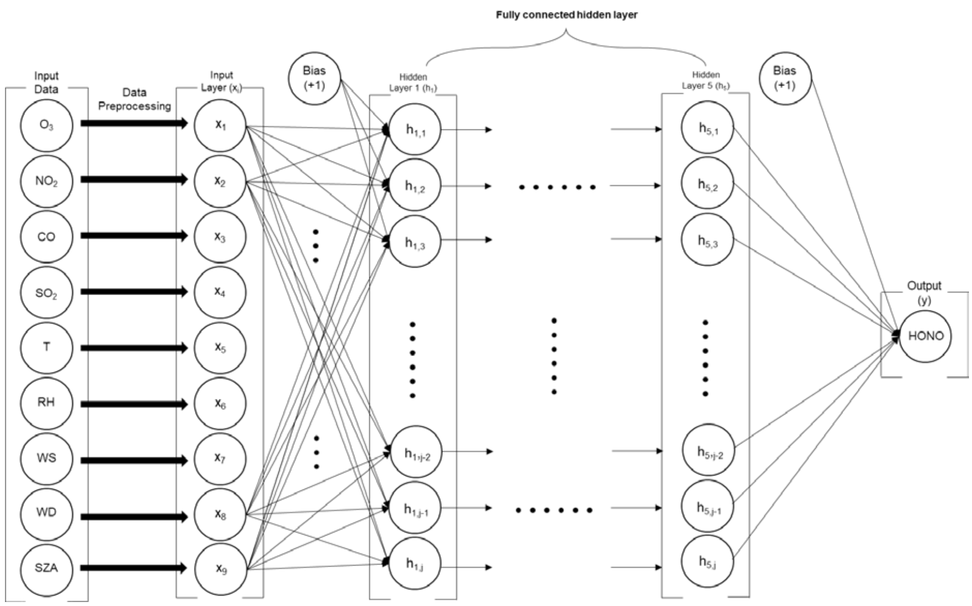

Figure 2. The structure of deep neural network built for RND v1.0.

https://doi.org/10.5194/gmd-2021-347
Preprint. Discussion started: 10 December 2021

Geoscientific Model Development
Discussions
Open Access
EGU

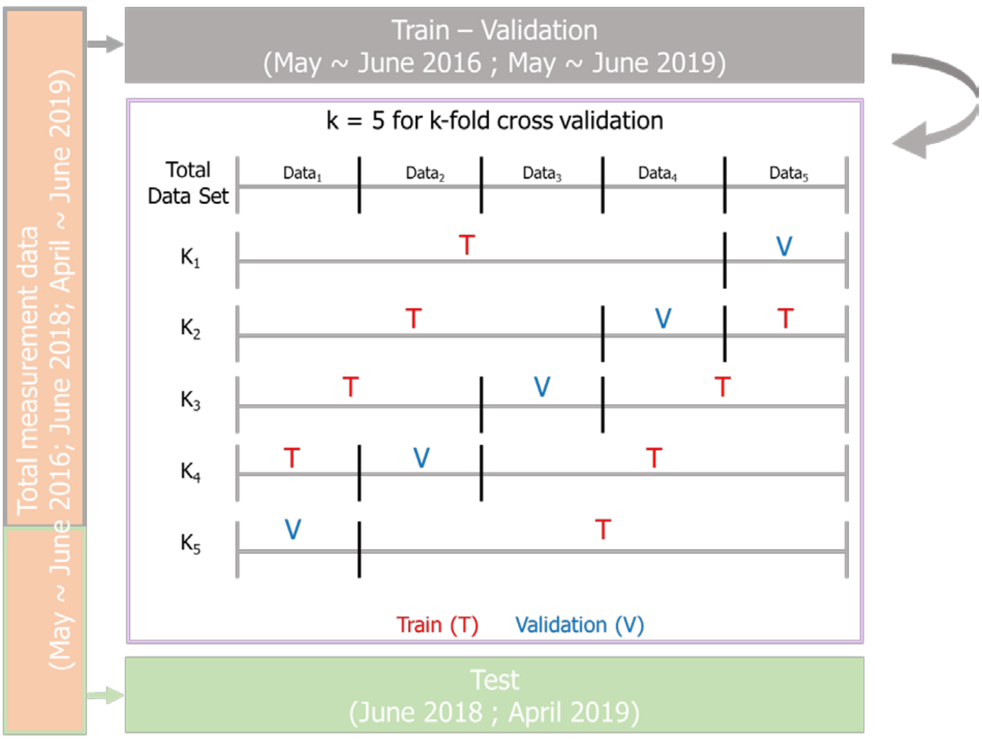

Figure 3. Design of training, validation, and test to build RNDv1.0 using measurement data. Training and validation were performed pairs using k-fold cross validation. Five subsets were randomly divided.

https://doi.org/10.5194/gmd-2021-347
Preprint. Discussion started: 10 December 2021

Geoscientific Model Development
Discussions

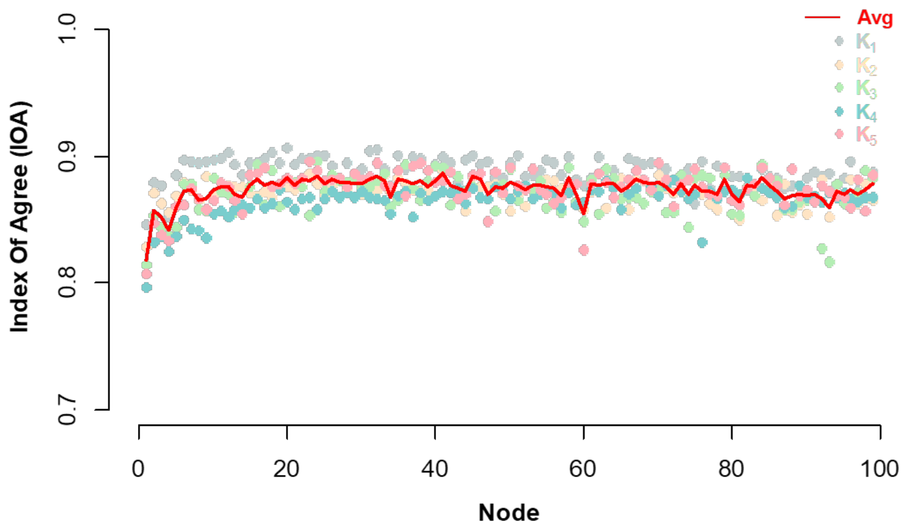

Figure 4. Index Of Agreement (IOA) for k-fold cross validation. Solid circle and red line represent IOA for each validation (k=5) and the average of 5 validation sets at each node number.

https://doi.org/10.5194/gmd-2021-347
Preprint. Discussion started: 10 December 2021

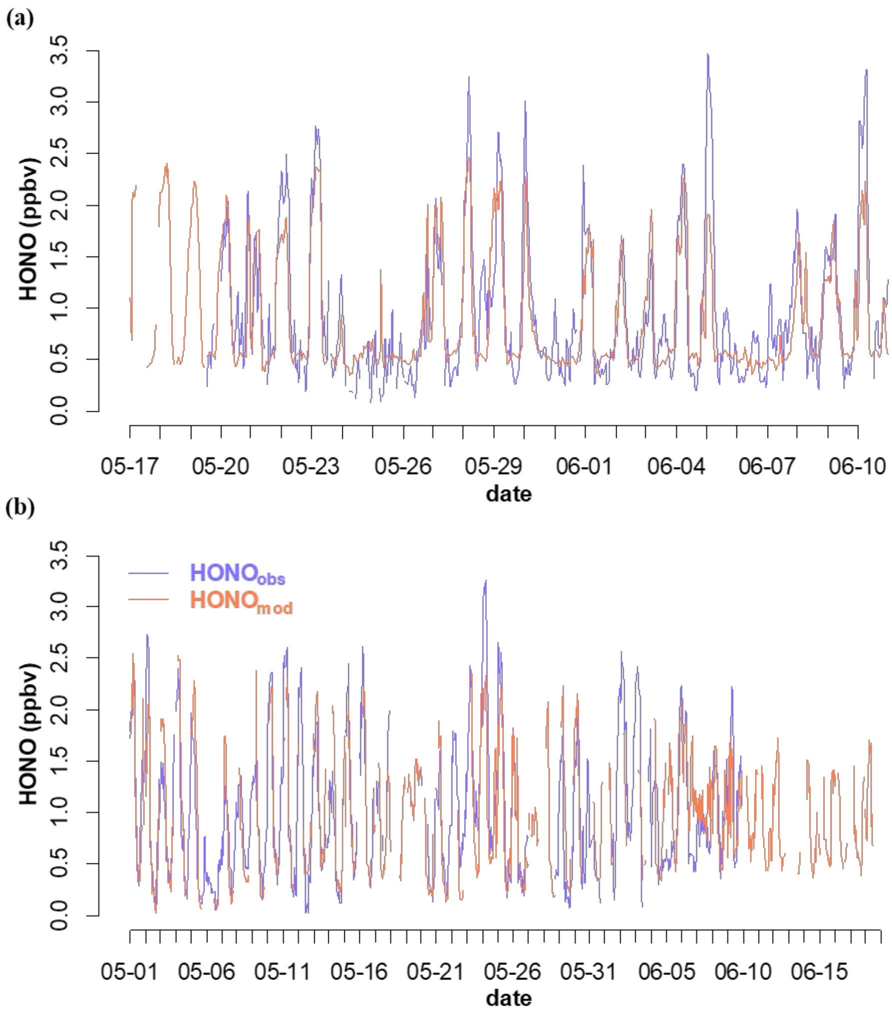

293

294 **Figure 5.** Comparison between the measured ($HONO_{obs}$) and calculated ($HONO_{mod}$) HONO
295 mixing ratios in Seoul during May~June in (a) 2016 and (b) 2019. The blue and red lines
296 indicate the measured and calculated HONO mixing ratio, respectively.

297

https://doi.org/10.5194/gmd-2021-347
Preprint. Discussion started: 10 December 2021

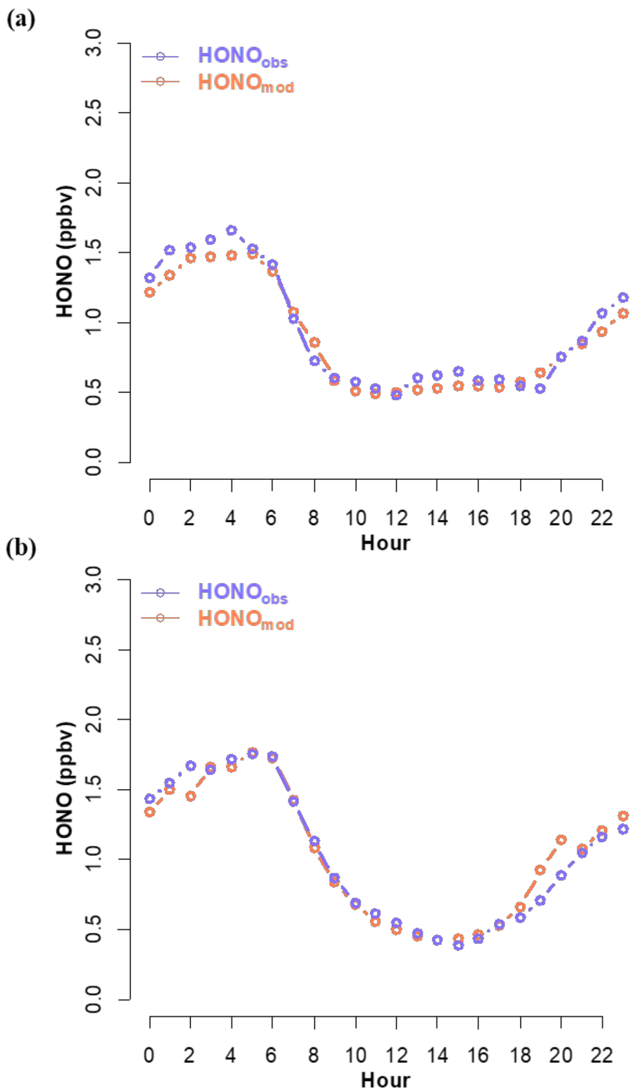

Figure 6. Average diurnal variations of the measured (HONO$_{obs}$) and the calculated (HONO$_{mod}$) HONO mixing ratios in Seoul during May ~ June in (a) 2016 and (b) 2019.

https://doi.org/10.5194/gmd-2021-347
Preprint. Discussion started: 10 December 2021

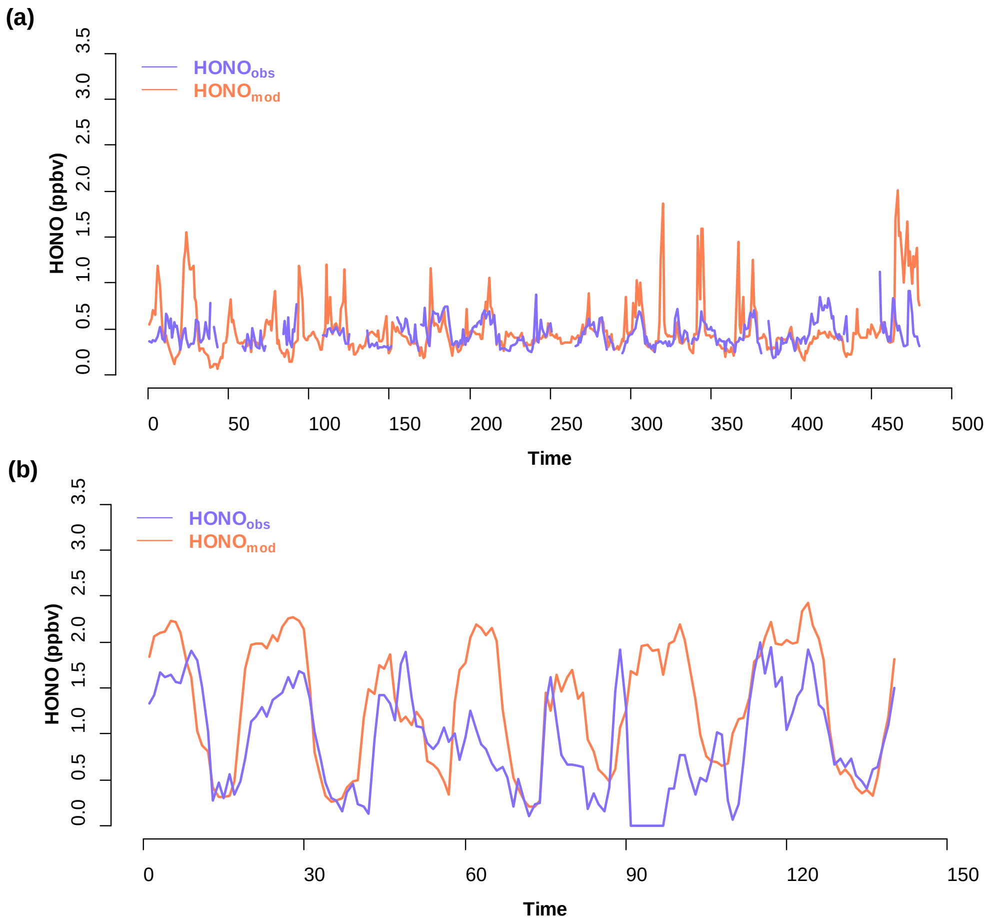

Figure 7. Comparison between the measured ($HONO_{obs}$) and calculated ($HONO_{mod}$) HONO mixing ratios in Seoul during (a) June 2018 and (b) April 2019. The blue and red lines indicate the measured and calculated HONO mixing ratio, respectively. The x axis indicates the hour from the beginning of the experiment, which is (a) 00:00 on 1st June 2018 and (b) 00:00 on 12th April 2019.

https://doi.org/10.5194/gmd-2021-347
Preprint. Discussion started: 10 December 2021

Geoscientific Model Development
Discussions

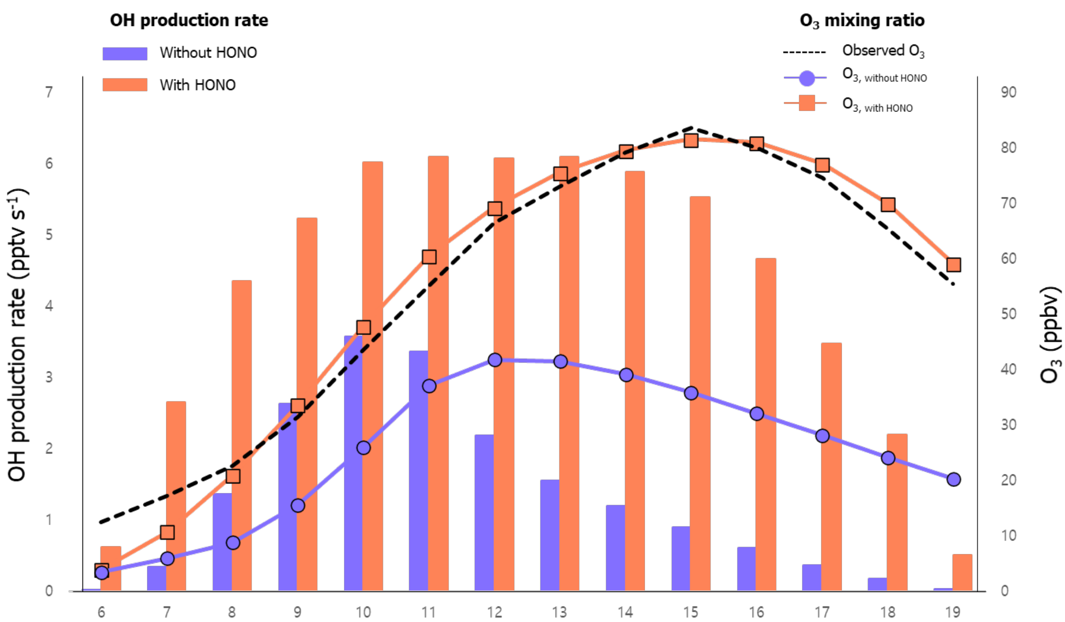

Figure 8. For June 2016, diurnal variations of O_3 (line) and OH production rate (bar) calculated from the F0AM photochemical model with (orange) and without (blue) HONO estimated from the RNDv1.0 model. The measured O_3 is compared with the calculated.

https://doi.org/10.5194/gmd-2021-347
Preprint. Discussion started: 10 December 2021

Table 1. Resources for constructing RND model.

	Version	Remark
Python	v3.8.3	
CUDA	v10.1	*If using GPU
CuDNN	v7.6.5	*If using GPU
Tensorflow	v2.3.0	*Python library*
Keras	v2.4.3	*Python library*
Pandas	v1.0.5	*Python library*
Numpy	v1.18.5	*Python library*

*GPU denotes graphic processing unit

https://doi.org/10.5194/gmd-2021-347
Preprint. Discussion started: 10 December 2021

Table 2. Input variables of the RNDv1.0 model and their ranges (10^{th} and 90^{th} percentile) observed in Seoul during May ~ June in 2016 and 2019.

	10^{th}~90^{th} percentile (unit)	Coverage (%)	Scale Factor1 (F_1)*	Scale Factor 2 (F_2)**
Input Variables				
O_3	12.1 ~ 90.4 (ppbv)	95.5	204.738	0.842
NO_2	11.0 ~ 48.6 (ppbv)	80.6	79.925	2.375
CO	252 ~ 743 (ppbv)	95.1	975.248	137.253
SO_2	1.9 ~ 6.4 (ppbv)	95.6	12.479	0.958
Solar Zenith Angle	22.7 ~ 118.4 (º)	100.0	112.317	14.195
Temperature	15.9 ~ 26.7 (°C)	99.4	24.240	8.610
Relative Humidity	29.2 ~ 79.1 (%)	99.4	88.545	10.555
Wind Speed	0.2 ~ 3.7 (m/s)	99.4	7.581	0.005
Wind Direction	45.4 ~ 287.5 (º)	99.4	359.565	0.235
Output Variables				
HONO	0.3 ~ 2.0 (ppbv)	81.1%	3.447	0.013

[*] Maximum – Minimum

[**] Minimum value

https://doi.org/10.5194/gmd-2021-347
Preprint. Discussion started: 10 December 2021

Geoscientific Model Development
Discussions
Open Access

Table 3. The result of validation and test of RNDv1.0 model using measurement data.

Measurement data	Validation		Test	
	MAE (ppbv)	IOA	MAE (ppbv)	MAE
May 2016	0.26	0.93		
June 2016	0.29	0.86		
June 2018			0.21	0.79
April 2019			0.56	0.65
May 2019	0.26	0.93		
June 2019	0.36	0.76		

https://doi.org/10.5194/gmd-2021-347
Preprint. Discussion started: 10 December 2021

Geoscientific Model Development Discussions

Reference

Alicke, B., Platt, U., and Stutz, J.: Impact of nitrous acid photolysis on the total hydroxyl radical budget during the Limitation of Oxidant Production/Pianura Padana Produzione di Ozono study in Milan, Journal of Geophysical Research: Atmospheres, 107, LOP 9-1-LOP 9-17, 2002.

Anderson, D. C., Loughner, C. P., Diskin, G., Weinheimer, A., Canty, T. P., Salawitch, R. J., Worden, H. M., Fried, A., Mikoviny, T., and Wisthaler, A.: Measured and modeled CO and NOy in DISCOVER-AQ: An evaluation of emissions and chemistry over the eastern US, Atmospheric Environment, 96, 78-87, 2014.

Bengio, Y., and Grandvalet, Y.: No unbiased estimator of the variance of K-fold cross-validation, Citeseer, 2003.

Brandenburger, U., Brauers, T., Dorn, H.-P., Hausmann, M., and Ehhalt, D. H.: In-situ measurements of tropospheric hydroxyl radicals by folded long-path laser absorption during the field campaign POPCORN, in: Atmospheric Measurements during POPCORN—Characterisation of the Photochemistry over a Rural Area, Springer, 181-204, 1998.

Brown, S. S., An, H., Lee, M., Park, J.-H., Lee, S.-D., Fibiger, D. L., McDuffie, E. E., Dubé, W. P., Wagner, N. L., and Min, K.-E.: Cavity enhanced spectroscopy for measurement of nitrogen oxides in the Anthropocene: results from the Seoul tower during MAPS 2015, Faraday discussions, 200, 529-557, 2017.

Chen, Y., Wolke, R., Ran, L., Birmili, W., Spindler, G., Schröder, W., Su, H., Cheng, Y., Tegen, I., and Wiedensohler, A.: A parameterization of the heterogeneous hydrolysis of N2O5 for mass-based aerosol models: improvement of particulate nitrate prediction, Atmos. Chem. Phys, 18, 673-689, 2018.

Cui, L., and Wang, S.: Mapping the daily nitrous acid (HONO) concentrations across China during 2006-2017 through ensemble machine-learning algorithm, Science of The Total Environment, 147325, 2021.

Ding, B., Qian, H., and Zhou, J.: Activation functions and their characteristics in deep neural networks, 2018 Chinese control and decision conference (CCDC), 2018, 1836-1841.

Ge, B., Xu, X., Ma, Z., Pan, X., Wang, Z., Lin, W., Ouyang, B., Xu, D., Lee, J., and Zheng, M.: Role of Ammonia on the Feedback Between AWC and Inorganic Aerosol Formation During Heavy Pollution in the North China Plain, Earth and Space Science, 6, 1675-1693, 2019.

Gil, J., Son, J., Kang, S., Park, J., Lee, M., Jeon, E., and Shim, M.: HONO measurement in Seoul during Summer 2018 and its Impact on Photochemistry, Journal of Korean Society for Atmospheric Environment, 36, 579-588, 10.5572/KOSAE.2020.36.5.579, 2020.

Gil, J.: RNDv1.0 and example, in, Zenodo, 2021.

Gil, J., Kim, J., Lee, M., Lee, G., Ahn, J., Lee, D. S., Jung, J., Cho, S., Whitehill, A., Szykman, J., and Lee, J.: Characteristics of HONO and its impact on O3 formation in the Seoul Metropolitan Area during the Korea-US Air Quality study, Atmospheric Environment, 2021, https://doi.org/10.1016/j.atmosenv.2020.118182., 2021.

Jordan, C., Crawford, J. H., Beyersdorf, A. J., Eck, T. F., Halliday, H. S., Nault, B. A., Chang, L.-S., Park, J., Park, R., Lee, G., Kim, H., Ahn, J.-y., Cho, S., Shin, H. J., Lee, J. H., Jung, J., Kim, D.-S., Lee, M., Lee, T., Whitehill, A., Szykman, J., Schueneman, M. K., Campuzano-Jost, P., Jimenez, J. L., DiGangi, J. P., Diskin, G. S., Anderson, B. E., Moore, R. H., Ziemba, L. D., Fenn, M. A., Hair, J. W., Kuehn, R. E., Holz, R. E., Chen, G., Travis, K., Shook, M., Peterson, D. A., Lamb, K. D., and Schwarz, J. P.: Investigation of factors controlling PM2.5 variability

https://doi.org/10.5194/gmd-2021-347
Preprint. Discussion started: 10 December 2021

across the South Korean Peninsula during KORUS-AQ, Elementa: Science of the Anthropocene, in review, 2020.

Kim, H., Gil, J., Lee, M., Jung, J., Whitehill, A., Szykman, J., Lee, G., Kim, D., Cho, S., Ahn, J., Hong, J., and Park, M.: Overview and characteristics of air quality in the Seoul Metropolitan Area during the KORUS-AQ campaign, Elementa: Science of the Anthropocene, in review, 2020.

Kleffmann, J., Lörzer, J., Wiesen, P., Kern, C., Trick, S., Volkamer, R., Rodenas, M., and Wirtz, K.: Intercomparison of the DOAS and LOPAP techniques for the detection of nitrous acid (HONO), Atmospheric Environment, 40, 3640-3652, 2006.

Lee, B. H., Wood, E. C., Zahniser, M. S., McManus, J. B., Nelson, D. D., Herndon, S. C., Santoni, G., Wofsy, S. C., and Munger, J. W.: Simultaneous measurements of atmospheric HONO and NO 2 via absorption spectroscopy using tunable mid-infrared continuous-wave quantum cascade lasers, Applied Physics B, 102, 417-423, 2011.

Levy, M., Zhang, R., Zheng, J., Zhang, A. L., Xu, W., Gomez-Hernandez, M., Wang, Y., and Olaguer, E.: Measurements of nitrous acid (HONO) using ion drift-chemical ionization mass spectrometry during the 2009 SHARP field campaign, Atmospheric Environment, 94, 231-240, 2014.

Li, Z., Xie, P., Hu, R., Wang, D., Jin, H., Chen, H., Lin, C., and Liu, W.: Observations of N2O5 and NO3 at a suburban environment in Yangtze river delta in China: Estimating heterogeneous N2O5 uptake coefficients, Journal of Environmental Sciences, 2020.

Liebmann, J., Karu, E., Sobanski, N., Schuladen, J., Ehn, M., Schallhart, S., Quéléver, L., Hellen, H., Hakola, H., and Hoffmann, T.: Direct measurement of NO3 radical reactivity in a boreal forest, Atmospheric Chemistry and Physics, 2018.

Liu, Y., Lu, K., Li, X., Dong, H., Tan, Z., Wang, H., Zou, Q., Wu, Y., Zeng, L., and Hu, M.: A comprehensive model test of the HONO sources constrained to field measurements at rural North China Plain, Environmental science & technology, 53, 3517-3525, 2019.

Peterson, D. A., Hyer, E. J., Han, S.-O., Crawford, J. H., Park, R. J., Holz, R., Kuehn, R. E., Eloranta, E., Knote, C., and Jordan, C. E.: Meteorology influencing springtime air quality, pollution transport, and visibility in Korea, Elem Sci Anth, 7, 2019.

Pinto, J., Dibb, J., Lee, B., Rappenglück, B., Wood, E., Levy, M., Zhang, R. Y., Lefer, B., Ren, X. R., and Stutz, J.: Intercomparison of field measurements of nitrous acid (HONO) during the SHARP campaign, Journal of Geophysical Research: Atmospheres, 119, 5583-5601, 2014.

Reichstein, M., Camps-Valls, G., Stevens, B., Jung, M., Denzler, J., and Carvalhais, N.: Deep learning and process understanding for data-driven Earth system science, Nature, 566, 195-204, 2019.

Roberts, J. M., Veres, P., Warneke, C., Neuman, J., Washenfelder, R., Brown, S., Baasandorj, M., Burkholder, J., Burling, I., and Johnson, T. J.: Measurement of HONO, HNCO, and other inorganic acids by negative-ion proton-transfer chemical-ionization mass spectrometry (NI-PT-CIMS): Application to biomass burning emissions, Atmospheric Measurement Techniques, 3, 981, 2010.

Ryan, R. G., Rhodes, S., Tully, M., Wilson, S., Jones, N., Frieß, U., and Schofield, R.: Daytime HONO, NO 2 and aerosol distributions from MAX-DOAS observations in Melbourne, Atmospheric Chemistry and Physics, 18, 13969-13985, 2018.

Sun, Y., Wang, L., Wang, Y., Quan, L., and Zirui, L.: In situ measurements of SO2, NOx, NOy, and O3 in Beijing, China during August 2008, Science of the Total Environment, 409, 933-940, 2011.

VandenBoer, T., Markovic, M., Sanders, J., Ren, X., Pusede, S., Browne, E., Cohen, R., Zhang, L., Thomas, J., and Brune, W. H.: Evidence for a nitrous acid (HONO) reservoir at the ground

https://doi.org/10.5194/gmd-2021-347
Preprint. Discussion started: 10 December 2021

surface in Bakersfield, CA, during CalNex 2010, Journal of Geophysical Research: Atmospheres, 119, 9093-9106, 2014.

Wang, H., Chen, X., Lu, K., Hu, R., Li, Z., Wang, H., Ma, X., Yang, X., Chen, S., and Dong, H.: NO3 and N2O5 chemistry at a suburban site during the EXPLORE-YRD campaign in 2018, Atmospheric Environment, 224, 117180, 2020.

Wang, T., Qin, Z., and Zhu, M.: An ELU network with total variation for image denoising, International Conference on Neural Information Processing, 2017a, 227-237.

Wang, X., Wang, H., Xue, L., Wang, T., Wang, L., Gu, R., Wang, W., Tham, Y. J., Wang, Z., and Yang, L.: Observations of N2O5 and ClNO2 at a polluted urban surface site in North China: High N2O5 uptake coefficients and low ClNO2 product yields, Atmospheric environment, 156, 125-134, 2017b.

Wolfe, G. M., Marvin, M. R., Roberts, S. J., Travis, K. R., and Liao, J.: The framework for 0-D atmospheric modeling (F0AM) v3. 1, Geoscientific Model Development, 9, 3309, 2016.

Xing, L., Wu, J., Elser, M., Tong, S., Liu, S., Li, X., Liu, L., Cao, J., Zhou, J., and El-Haddad, I.: Wintertime secondary organic aerosol formation in Beijing–Tianjin–Hebei (BTH): contributions of HONO sources and heterogeneous reactions, Atmospheric Chemistry & Physics, 19, 2019.

Xu, Z., Liu, Y., Nie, W., Sun, P., Chi, X., and Ding, A.: Evaluating the measurement interference of wet rotating-denuder–ion chromatography in measuring atmospheric HONO in a highly polluted area, Atmospheric Measurement Techniques, 12, 6737-6748, 2019.

Xue, C., Ye, C., Ma, Z., Liu, P., Zhang, Y., Zhang, C., Tang, K., Zhang, W., Zhao, X., and Wang, Y.: Development of stripping coil-ion chromatograph method and intercomparison with CEAS and LOPAP to measure atmospheric HONO, Science of The Total Environment, 646, 187-195, 2019.

Xue, C., Zhang, C., Ye, C., Liu, P., Catoire, V., Krysztofiak, G., Chen, H., Ren, Y., Zhao, X., and Wang, J.: HONO budget and its role in nitrate formation in the rural North China Plain, Environmental Science & Technology, 54, 11048-11057, 2020.

Ye, C., Zhou, X., Pu, D., Stutz, J., Festa, J., Spolaor, M., Tsai, C., Cantrell, C., Mauldin, R. L., and Campos, T.: Rapid cycling of reactive nitrogen in the marine boundary layer, Nature, 532, 489-491, 2016.